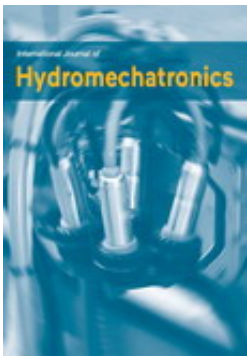

International Journal of Hydromechatronics

ISSN online: 2515-0472 - ISSN print: 2515-0464
https://www.inderscience.com/ijhm

Robust active disturbance rejection control for modular fluidic soft actuators

Yunce Zhang, Tao Wang, Xuqu Hu

DOI: 10.1504/IJHM.2023.10059853

Article History:

Received:	18 March 2023
Last revised:	28 May 2023
Accepted:	01 June 2023
Published online:	06 December 2024

Robust active disturbance rejection control for modular fluidic soft actuators

Yunce Zhang

Ocean College,
Zhejiang University,
Zhoushan 316000, China
and
Inspur Academy of Science and Technology,
Jinan 250000, China
Email: yc_zhang@zju.edu.cn

Tao Wang*

Ocean College,
Zhejiang University,
Zhoushan 316000, China
Email: twang001@zju.edu.cn
and
Research Center of Oceanic Sensing Technology and Equipment,
Ministry of Education, China
*Corresponding author

Xuqu Hu

Biomechanics and Bioengineering Laboratory (UMR CNRS 7338),
Université de Technologie de Compiègne,
Alliance Sorbonne Université,
60203 Compiègne, France
and
Life Science Technologies Department,
Imec, Leuven, Belgium
Email: huxuqu@gmail.com

Abstract: Delicate dynamic control of soft actuators is a challenging task due to their strongly nonlinearities. This article focuses on the dynamic control of the modular fluidic soft actuators governed by pneumatic proportional valves. Since it is difficult to accurately describe the complex coupling relationships among the chambers of the soft actuators, the dynamic control of the soft actuators cannot be implemented by using advanced control algorithms based on precise model in usual. To improve the manipulability and extend the application scenarios, we design a robust active disturbance rejection control method based on linear extended state observer, which only requires an approximate model of the soft actuators. Experimental results show that closed-loop stability and good tracking performance are achieved by the

proposed method, meanwhile better disturbance rejection ability is guaranteed in comparison to the commonly used proportional-integral-differential control method.

Keywords: controller design; state observation; dynamic performance; fluidic power; modular soft actuators.

Reference to this paper should be made as follows: Zhang, Y., Wang, T. and Hu, X. (2024) 'Robust active disturbance rejection control for modular fluidic soft actuators', *Int. J. Hydromechatronics*, Vol. 7, No. 4, pp.293–309.

Biographical notes: Yunce Zhang received his PhD degree in Mechanical Engineering from Ocean College, Zhejiang University, Zhoushan, China, in 2022. Currently, he is an artificial intelligence researcher at Inspur Academy of Science and Technology, Jinan, China. His research interests include soft robotics and digital twin.

Tao Wang received his BS and PhD degrees in Mechanical Engineering from Zhejiang University, Hangzhou, China in 2008 and 2013, respectively. Currently, he is an Associate Professor at the Ocean College, Zhejiang University, Zhoushan, China. His research interests include mechatronic system and robotics.

Xuqu Hu received his PhD degree in Biomechanics and Bioengineering from Universite de Technologie de Compigne (France) in 2013. He was a researcher in the French National Centre for Scientific Research (CNRS). He is currently a permanent senior researcher in the Interuniversitair Micro-Electronica Centrum vzw (IMEC) in Belgium.

This paper is a revised and expanded version of a paper entitled 'Robust active disturbance rejection control for modular fluidic soft actuators' presented at 24th International Conference of Fluid Power and Mechatronic Control Engineering, Taiyuan, China, August 2023.

1 Introduction

Inspired by the structure and motion mechanism of natural soft biological systems, soft robots have received extensive attention and a lot of researches as an emerging cross-field. Soft robots have advanced characteristics of inherent compliance, environmental adaptability, and low inertia (Rus and Tolley, 2015; Roderick et al., 2021), which provide promising prospects in the applications of human–machine interactions and unstructured environments (Wang et al., 2019b; Shengda et al., 2021), such as flexible manipulation (Abondance et al., 2020; Kurumaya et al., 2018), bionic locomotion (Zhang et al., 2022; Zou et al., 2018), minimally invasive surgery (Cianchetti et al., 2014; Abidi et al., 2018), and rehabilitation (Maeder-York et al., 2014; Chu, 2018). With the development of the soft robots, amounts of actuation methods have been applied, such as fluidic actuation (Marchese et al., 2015b; Feng et al., 2020), shape memory alloy actuation (Laschi et al., 2012; Villanueva et al., 2011), cable-driven actuation (Xu et al., 2018; Renda et al., 2014), combustion actuation (Shepherd et al., 2013; 20 Truby and Li, 2020), ionic polymer metal composite actuation (Shen et al., 2013; Li et al., 2016) and so on. Due to the advantages of the fluidic actuation, like high power density (Li et al.,

2019; Zhang et al., 2023), low material cost and ease of manufacture, it becomes the most widely used actuation method for multi-degree-of-freedom (multi-DOF) soft robots (Marchese et al., 2015a; Wang et al., 2019a).

Although the materials, structures and actuation methods of the multi-DOF soft robots have been significantly developed in the past decades, the delicate dynamic control is still a challenging task which requires to be well explored and analysed due to the strongly nonlinearities and redundant DOFs (Zongxing et al., 2020; Zhou et al., 2022). Without the advanced control ability, soft robots can only achieve simple forms of manipulation and locomotion, or realise specific tasks by increasing the structural complexity (Lee et al., 2017; Wang et al., 2022a).

According to the review of literatures, common control methods of fluidic soft robots can be categorised into two types, the model-based methods and the model-free methods. The model describing the relationships between the chamber pressures and the actuator deformation should be developed firstly when using the model-based methods (Wang et al., 2022b; Wang and Zhang, 2022). An accurate model or a reasonably simplified model is the guarantee of good control performance (Wen et al., 2023). For example, a kinematic model of the soft robotic arm developed by using DH parameters is used to achieve close-loop control (Ohta et al., 2018; Huang et al., 2022). To improve the solving efficient, a simple and rapid inverse kinematics method is proposed to control the spatial location and trajectory of the underwater soft manipulator's end effector (Gong et al., 2020). In order to further exploit the rich dynamics of the soft robots, some studies pay attention to the dynamic model. A dynamic model of a soft continuum robotic arm is built by using a rigorous geometrically exact method (Renda et al., 2014). Based on the simplified dynamics, a nonlinear robust control algorithm is developed for soft bending actuator by backstepping design method to deal with nonlinearities and uncertainties (Wang et al., 2019a). Generally, it is complex and difficult to accurately model the multi-DOF soft actuator due to the nonlinearity and viscoelastic effect of soft materials. Therefore, the model-based methods which strongly rely on the accurate model are unsuitable to achieve guaranteed dynamic control performance of the soft actuators in the presence of complex coupling effect and external disturbances.

In contrast, the model-free methods provide an alternative solution for the control of the soft robots without modelling. For instance, a cascaded control structure based on proportional-integral-differential (PID) controller is designed to control soft robotic manipulation system (Marchese and Rus, 2015; Marchese et al., 2014). To improve control performance on spatial continuum arm, a model-free approach based on deep reinforcement learning is proposed by using Deep-Q Learning with experience replay to train the control system (Satheeshbabu et al., 2019). The recurrent neural network is also used to represent the dynamic model of the soft robot, and the closed-loop policy can be derived using trajectory optimisation and supervised learning based on the model (Thuruthel et al., 2019). Although the learning-based methods can realise motion control, they still have certain limitations in the application of multi-DOF soft actuators due to the large amount of sample data and computing resources required.

In general, it is difficult to obtain the complete dynamic information of the soft robots, but part of them can be obtained. Aforementioned model-free methods do not make good use of this known information, and cannot quickly decrease the effects of disturbances. To improve the disturbances rejection ability and make better use of known information, Han proposes the active disturbance rejection control (ADRC) control method (Han, 2009), which has been verified on various plants. Li et al. (2021)propose a

hand rehabilitation device and use the ADRC algorithm to achieve the control purpose. An ADRC combined with fuzzy algorithm is also designed for a variable-stiffness soft arm to adjust the parameters of the ADRC and control stiffness and position of the soft arm (Hao et al., 2018). Overall, the ADRC method has low requirements on the accuracy of the plant model. It observes un-modelled dynamics and external disturbances as total disturbances based on partially known dynamics and extended state observer (ESO), and performs real-time compensation to eliminate the influence of disturbance (Fareh et al., 2021; Zheng and Gao, 2018). There, it can be deduced that the ADRC methods are especially suitable for the fluidic multi-DOF soft actuators with strongly nonlinearities and disturbances. However, the current researches of ADRC on soft robots are mostly about relatively simple motions, and the ADRC of soft robots with multi-DOF and complex spatial motions are still in their nascent stage.

In this paper, we investigate the dynamic control of the modular fluidic soft actuators with multi-DOF, which can be quickly assembled into a variety of soft robots by using magnets (Kwok et al., 2014). We keep parts of the dynamic model parameters which depend on the structural parameters of the soft actuators, and treat the rest as disturbances uniformly. Based on the simplified dynamics, a linear extended state observer (LESO) is developed to observe the system states and total disturbances expanded to the system state. We convert the system to a series of standard integrators by performing real-time compensation for total disturbances. To reduce the influence of model uncertainty on the stability of the closed-loop system and achieve good dynamic control performance, a robust controller is designed based on the philosophy of ADRC, which can realise the ADRC of the soft actuators. To validate the effectiveness of the proposed control method, an experimental platform is built with actuation system and visual measurement system. The experimental results show that the closed-loop stability and the good tracking performance are achieved by the proposed method, and better disturbance rejection ability is guaranteed compared to the commonly used PID control method. The main contributions of this work are summarised as follows.

- A successful attempt of the ADRC method based on the combination of a LESO and a robust controller in a multi-DOF soft robot to achieve complex spatial motion.
- Experimental verification of the proposed method to demonstrate its effectiveness of controlling the soft robot under disturbance.

Table 1 The key parameters of fluidic soft actuators

Parameter	*Value*	*Unit*
Reference radius of chambers	5	mm
Initial length of chambers	60	mm
Inner diameter of chambers	3	mm
Outer diameter of chambers	5	mm
Outer diameter	20	mm
Initial length	60	mm
Maximum pressure	400	kPa

2 System description

2.1 Hardware of control system

The studied modular fluidic soft actuator is shown in Figure 1. It mainly consists of a soft cylindrical body, two connectors with embedded magnets, and three fibre-reinforced fluidic chambers. A secondary casting process is employed to form an elastic cylinder that wraps the chambers, which is important to prevent buckling.

Figure 1 Studied modular fluidic soft actuator, (a) schematic diagram of soft actuator structural components, (b) soft actuator prototype (see online version for colours)

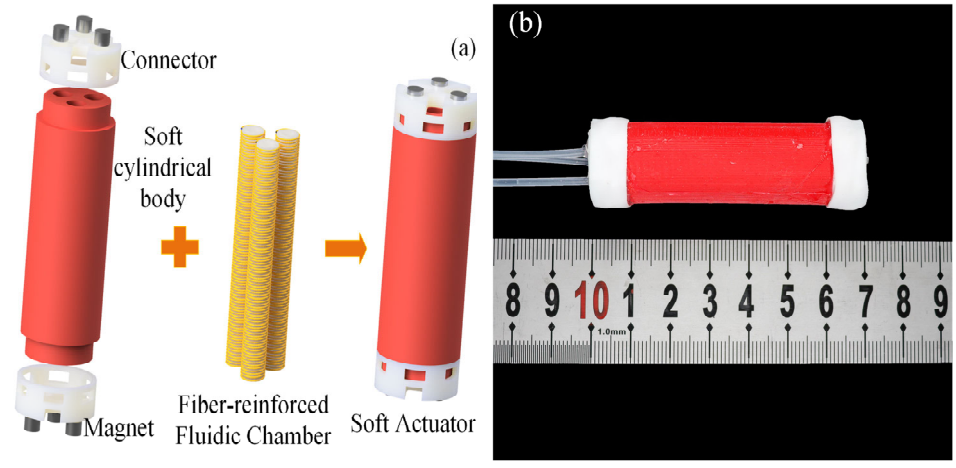

The soft actuator can be operated with multiple DOFs by controlling the pressure distribution in the three chambers. The key parameters of the soft actuator are listed in Table 1. The reference radius of chambers is the distance from the central axis of the soft actuator to the central axis of any chamber.

A pneumatic control system with proportional solenoid valves is designed to actuate and control the soft actuator, as shown in Figure 2. After experimental tests, the maximum pressure of the soft actuator developed in this paper is 400 kPa. When actuating a single channel to bend the soft actuator to 90 degrees, its working pressure is about 150 kPa. Therefore, the reasonable design of the drive system should consider the actual working pressure range of the soft actuator, and leave some redundancy. Considering the small actual volume of the soft actuator and the high requirements for the integration of the experimental platform, the ITV1050-312L proportional valves produced by SMC company from Japan are used as the basic driving unit of the driving system to reduce the number of components and improve system integration. Pressure sensors (PSE574-10, SMC, Japan Inc.) are utilised to measure the fluidic pressures in the chambers of the modular fluidic soft actuators. A data acquisition device (Q8-USB, Quanser, Canada Inc.) is used to collect the pressure data and supply control signals to the proportional solenoid valves.

To measure the coordinates of the joints of the soft actuator, a stereo camera ZED2 (Stereolabs, USA Inc.) is deployed to build a visual measurement system. Before measuring, the parameters of the stereo camera need to be calibrated first, because the

calibration result has a great influence on the measurement accuracy. The ZED2 stereo camera has undergone a rigorous calibration process when it leaves the factory. However, the distortion parameters of the camera and the relative exchange relationship between the two cameras will change to a certain extent in underwater measurement. Therefore, it is necessary to re-calibrate the internal and external parameters of the camera underwater.

Figure 2 Schematic of control system for modular fluidic soft actuators (see online version for colours)

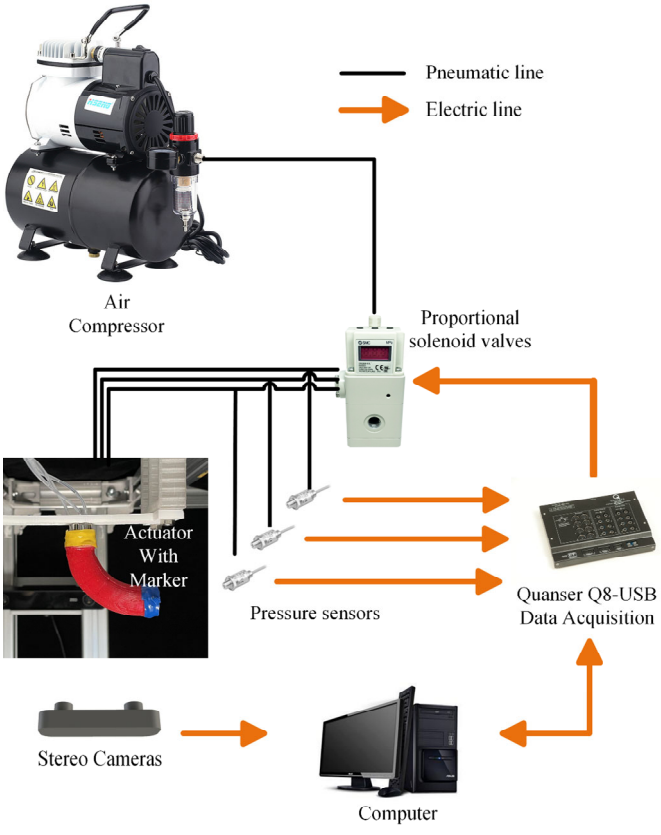

The camera calibration process is carried out in MATLAB, which is mainly divided into three steps: image acquisition, monocular camera calibration and binocular camera calibration. The calibration plate is made of glass panel with alumina material (GP290, Chenzheng Precision Co., Ltd., China). The dimensions are 290 mm high and 230 mm wide, with an accuracy of 0.01 mm and a low thermal expansion coefficient. When collecting images in the water, the position of the calibration plate was constantly changed, and 33 pictures of the left camera and the right camera are taken for calibration. Finally, the calibration parameters of the monocular camera and stereo camera are determined successively by using the camera calibration toolboxes of MATLAB. After calibration, the accuracy of the depth camera is evaluated, and the average error in the measurement range is about 7 mm.

The SDK development tools for the ZED2 camera provide RGB images and point clouds. Therefore, the target position measurement can be done by first extracting the centre point of the region of interest from the RGB image using the OpenCV library, and then obtaining the three-dimensional information of the centre point from the corresponding point clouds.

In measuring, firstly, some labels are set at the joints of the soft actuator to facilitate the subsequent identification of the corresponding joints through the classical image segmentation algorithm. The three-dimensional coordinates of each joint are subtracted from its three-dimensional coordinate value in the stereo camera coordinate system by the coordinate value of the base point of the soft actuator. By introducing the three-dimensional coordinates of each joint to the kinematic model (Xie et al., 2020a), the lengths of each chamber of the soft actuator can be calculated respectively.

2.2 Dynamic model of soft actuators

When the chambers are stretched by the pressurised fluid, the surrounding soft cylindrical body also extends, and the dynamic equation can be written as (Xie et al., 2020b)

$$\begin{cases} \dfrac{m\ddot{l}_{i1}}{3}+\dfrac{(-m+\rho V)g}{2}+\pi\mu(R^2-r^2)\left(\dfrac{l_{i1}}{l_0}-\dfrac{l_0^3}{l_{i1}^3}\right)+C_v\dot{l}_1=\pi r^2P_{i1} \\ \dfrac{m\ddot{l}_{i2}}{3}+\dfrac{(-m+\rho V)g}{2}+\pi\mu(R^2-r^2)\left(\dfrac{l_{i2}}{l_0}-\dfrac{l_0^3}{l_{i2}^3}\right)+C_v\dot{l}_2=\pi r^2P_{i2} \\ \dfrac{m\ddot{l}_{i3}}{3}+\dfrac{(-m+\rho V)g}{2}+\pi\mu(R^2-r^2)\left(\dfrac{l_{i3}}{l_0}-\dfrac{l_0^3}{l_{i3}^3}\right)+C_v\dot{l}_3=\pi r^2P_{i3} \end{cases} \tag{1}$$

where m is the weight of the chamber, ρ is the density of water, μ is the initial shear modulus of the material, V is the volume of chamber, g is the gravitational acceleration, l_0 is the initial length, l_{ij} (j = 1, 2, 3) and P_{ij} (j = 1, 2, 3) correspond to the three chambers of the soft actuator, R is the outer radius of the chamber, r is the inner radius, and C_v is the damping coefficient.

Based on (1), we can calculate the lengths of the chambers with the input pressure and initial state. Furthermore, we can obtain the joint variables of the soft actuator according to constant curvature assumption as

$$\begin{cases} l_i=\dfrac{l_{i1}+l_{i2}+l_{i3}}{3} \\ \theta_i=\dfrac{2\sqrt{l_{i1}^2+l_{i2}^2+l_{i3}^2-l_{i1}l_{i2}-l_{i1}l_{i3}-l_{i2}l_{i3}}}{3d} \\ \varphi_i=\tan^{-1}\left(\dfrac{l_{i2}+l_{i3}-2l_{i1}}{\sqrt{3}(l_{i2}-l_{i3})}\right) \end{cases} \tag{2}$$

where d is the distance between the centre of chamber and the centre of the soft actuator. The transformation matrix from joint variables to Cartesian coordinates can be derived as

$$\mathbf{T_i} = \begin{bmatrix} \mathbf{R_z}(\varphi_i) & 0 \\ 0 & 1 \end{bmatrix} \begin{bmatrix} \mathbf{R_y}(\theta_i) & \mathbf{p} \\ 0 & 1 \end{bmatrix} \begin{bmatrix} \mathbf{R_z}(-\varphi_i) & 0 \\ 0 & 1 \end{bmatrix}$$

$$= \begin{bmatrix} c^2\varphi_i\, c\theta_i + s^2\varphi_i & c\theta_i\, s\varphi_i\,(c\theta_i - 1) & c\varphi_i\, s\theta_i & \dfrac{l_i\, c\varphi_i\,(1 - c\theta_i)}{\theta_i} \\ c\varphi_i\, s\varphi_i\,(c\theta_i - 1) & s^2\varphi_i\, c\theta_i + c^2\varphi_i & s\varphi_i\, s\theta_i & \dfrac{l_i\, s\varphi_i\,(1 - c\theta_i)}{\theta_i} \\ -c\varphi_i\, s\theta_i & -s\varphi_i\, s\theta_i & c\theta_i & \dfrac{l_i\, s\theta_i}{\theta_i} \\ 0 & 0 & 0 & 1 \end{bmatrix} \tag{3}$$

where $c\varphi_i = c\theta_i = \cos\theta_i$, $s\varphi_i = \sin\varphi_i$, $s\theta_i = \sin\theta_i$. If the two-segment tandem actuators are deployed, the transformation matrix from joint variables to Cartesian coordinates can be derived following (2) and (3) as

$$\mathbf{T} = \mathbf{T_1}\mathbf{T_2} \tag{4}$$

3 Control method

3.1 Problem formulation

Since the material density of the soft actuator is close to water, it is reasonably assumed that the buoyancy of the soft actuator is equal to the gravity. The dynamics of the chamber can be rewritten as

$$\ddot{y}(t) = -a_0 y(t) - a_1 y^{-1}(t) - a_1 \dot{y}(t) + \delta(t) + bu(t) = f(t) + bu(t) \tag{5}$$

where $y(t)$ is the length of the soft actuator, $\delta(t)$ is the external disturbance, $u(t)$ is the control input, i.e., the fluid pressure. Since there are errors between the identified system parameters and the actual system parameters, we treat all parts other than the control input as total disturbance defined as $f(t)$, including un-modelled dynamics, parameter uncertainties, and external disturbances.

It is noted that the parameter b should be equal or close to the true value to make the LESO work properly. Although b is the theoretical value from dynamics in our application and may be different from the actual value of the system, the error of b can be treated as a part of total disturbance. As long as b does not deviate much from the actual value, the LESO can work normally, and the dynamic control performance of the proposed controller can still be guaranteed.

3.2 LESO design

Select the state variables $x_1(t) = l$, $x_2(t) = \dot{l}$, $x_3(t) = f$, thus $\mathbf{x(t)} = [x_1(t)\ x_2(t)\ x_3(t)]$ is the extended state including total disturbance. So, the chamber dynamics can be rewritten in state-space form as

$$\begin{cases} \dot{\mathbf{x}}(\mathbf{t}) = \mathbf{A}\mathbf{x}(\mathbf{t}) + \mathbf{B}u(t) + \mathbf{E}\dot{f}(t) \\ y(t) = \mathbf{C}\mathbf{x}(\mathbf{t}) \end{cases} \tag{6}$$

where $\mathbf{A}=\begin{bmatrix}0 & 1 & 0\\ 0 & 0 & 1\\ 0 & 0 & 0\end{bmatrix}$, $\mathbf{B}=\begin{bmatrix}0\\ b\\ 0\end{bmatrix}$, $\mathbf{E}=\begin{bmatrix}0\\ 0\\ 1\end{bmatrix}$, $\mathbf{C}=\begin{bmatrix}1 & 0 & 0\end{bmatrix}$

The LESO used to estimate the total disturbance can be constructed as

$$\begin{cases}\dot{\mathbf{z}}(\mathbf{t})=\mathbf{A}\mathbf{z}(\mathbf{t})+\mathbf{B}u(t)+\mathbf{L}\left(y(t)-\mathbf{C}\mathbf{z}(\mathbf{t})\right)\\ \mathbf{y_c}(\mathbf{t})=\mathbf{z}(\mathbf{t})\end{cases} \tag{7}$$

where $\mathbf{z(t)}$ = $[z_1(t)\ldots z_2(t)\ldots z_3(t)]$ is the state vector of the observer, $z_1(t)=\hat{x}_1(t), z_2(t)=\hat{x}_2(t),$ and $z_3(t)=\hat{x}_3(t)$. $\mathbf{L}$ = $[l_1\ldots l_2\ldots l_3]$ is the gain vector to be designed for the observer, and $\mathbf{y_c(t)}$ is the outputs of the LESO.

To quickly configure the gain vector of the observer, the poles of the characteristic equation can be placed in the same location ω_0, which is the bandwidth of the observer (Gao, 2003). The characteristic equation is written as

$$\lambda(s)=\left|sI-(A-LC)\right|=\left(s+\omega_o\right)^3 \tag{8}$$

So, the gain vector of the observer can be configured as

$$\mathbf{L}=\begin{bmatrix}3\omega_o & 3\omega_o^2 & \omega_o^3\end{bmatrix}^{\mathrm{T}} \tag{9}$$

Let $\tilde{x}=x-z$ be the estimation error of the observer, the estimation error dynamics can be written as

$$\dot{\tilde{\mathbf{x}}}(\mathbf{t})=\mathbf{A}_{\tilde{\mathbf{x}}}\tilde{\mathbf{x}}(\mathbf{t})+\mathbf{E}\dot{f}(t) \tag{10}$$

where $\tilde{\mathbf{x}}(\mathbf{t})=\left[\tilde{x}_1(t)\ \tilde{x}_2(t)\ \tilde{x}_3\ (t)\right]$, $\tilde{x}_1(t)=x_1(t)-z_1(t)$, $\tilde{x}_2(t)=x_2(t)-z_2(t)$, $\tilde{x}_3(t)=x_3(t)-z_3(t)$, and $\mathbf{A}_{\tilde{\mathbf{x}}}=\mathbf{A}-\mathbf{LC}=\begin{bmatrix}-3\omega_0 & 1 & 0\\ -3\omega_0^2 & 0 & 1\\ -\omega_0^3 & 0 & 0\end{bmatrix}$.

Assumption 1: The derivative of the total disturbance is bounded as follows

$$\sup_{t\in[t_0,\infty)}\left\|\dot{f}\right\|\le\varepsilon \tag{11}$$

where ε is the upper bound which can be arbitrarily small.

Theorem 1: The ultimate upper bound of the disturbance estimation is $\limsup_{t\to\infty}\left|\tilde{x}_3(t)\right|\le\frac{2\varepsilon}{\omega_0}+\frac{2\varepsilon}{\omega_0^2}+\frac{2\varepsilon}{\omega_0^3}$

Proof: Based on the observation error dynamics defined in (10), it can be calculated as

$$
\begin{aligned}
\left\|\tilde{x}(t)\right\| &= \left\| e^{A_{\tilde{x}}t}\tilde{x}(0) + \int_0^t e^{A_{\tilde{x}}(t-\tau)}E\dot{f}(\tau)d\tau \right\| \\
&\le \left\| e^{-\omega_0 t}\begin{bmatrix} \frac{t^2}{2}+2t+1 & \frac{t^2}{2\omega_0}-\frac{t}{\omega_0} & \frac{t^2}{2\omega_0^2} \\ \omega_0 t^2+3\omega_0 t & -t^2-t+1 & \frac{t^2}{\omega_0}-\frac{t}{\omega_0} \\ \frac{\omega_0^2 t^2}{2}+\omega_0^2 t & -\frac{\omega_0 t^2}{2} & \frac{t^2}{2}-t+1 \end{bmatrix}\begin{bmatrix} 0 \\ 0 \\ \tilde{x}_3(0) \end{bmatrix} \right\| \\
&\quad -\varepsilon\int_0^t\left(1+\frac{1}{\omega_0}\right)(t-\tau)e^{-\omega_0(t-\tau)}d\tau + \varepsilon\int_0^t \frac{1+2\omega_0+\omega_0^2}{2\omega_0^2}(t-\tau)^2 e^{-\omega_0(t-\tau)}d\tau \\
&\quad +\varepsilon\int_0^t e^{-\omega_0(t-\tau)}d\tau \le \left\|\tilde{x}_3(0)\right\|\left(\frac{t^2}{2\omega_0^2}+\frac{t^2}{\omega_0}-\frac{t}{\omega_0}+\frac{t^2}{2}-t+1\right)e^{-\omega_0 t} \\
&\quad +\varepsilon\left[\frac{(1+\omega_0)(\omega_0 t+1)}{\omega_0}-\frac{1}{\omega_0}\right]e^{-\omega_0 t} - \varepsilon\left[\frac{\left(1+2\omega_0+\omega_0^2\right)}{2\omega_0^5}\left(\omega_0^2 t^2+w\omega_0 t+2\right)\right]e^{-\omega_0 t} \\
&\quad +\frac{2\varepsilon}{\omega_0}+\frac{2\varepsilon}{\omega_0^2}+\frac{2\varepsilon}{\omega_0^3}
\end{aligned}
\tag{12}
$$

Thus, the ultimate upper bound of the disturbance estimation error satisfies

$$
\limsup_{t\to\infty}\left|\tilde{x}_3(t)\right| \le \limsup_{t\to\infty}\left|\tilde{\mathbf{x}}(\mathbf{t})\right| \le \frac{2\varepsilon}{\omega_0}+\frac{2\varepsilon}{\omega_0^2}+\frac{2\varepsilon}{\omega_0^3} \tag{13}
$$

The system is compensated using the total disturbance observed by ESO and can be rewritten as

$$
\ddot{y}(t) = bu(t) - \tilde{x}_3(t) \tag{14}
$$

3.3 Robust controller design

Define the output tracking error function as

$$
e_2 = \dot{e}_1 + k_1 e_1 \tag{15}
$$

where $e_1 = x_1 – l_d$ is the output tracking error, and k_1 is any positive feedback gain. Thus, making e_1 small or concerge to zero is equivalent to making e_2 small or converge to zero.

The error dynamics can be obtained from (14) and (15) as

$$
\begin{aligned}
\dot{e}_2 &= \ddot{e}_1 + k_1\dot{e}_1 \\
&= bu + \tilde{x}_3 - \ddot{l}_d + k_1\left(\hat{x}_2+\tilde{x}_2\right) - k_1\dot{l}_d
\end{aligned}
\tag{16}
$$

Considering u_d as the virtual control input of u, the control law is designed as

$$
u_d = u_{da} + u_{ds1} + u_{ds2} \tag{17}
$$

where u_{da} and u_{ds1} are given as

$$\begin{cases} u_{da} = \dfrac{k_1 \dot{l}_d + \ddot{l}_d - k_1 \hat{x}_2}{\hat{b}} \\ u_{ds1} = -\dfrac{1}{b_{\min}} k_2 e_2 \end{cases} \tag{18}$$

where $\hat{b}$ is the identified value of model parameters in (14), b_{min} is the minimum bound of b, and k_2 is any positive feedback gain. The term u_{ds2} is a nonlinear feedback term, satisfying

$$e_2 \left(\mathbf{\Phi}^T \tilde{x} - \tilde{b} u_{da} + b u_{ds2} \right) \le \varepsilon_2 \tag{19}$$

where ε_2 is a positive design parameter which can be arbitrarily small. The parameter estimate error is defined as $\tilde{b} = \hat{b} - b,$ and $\mathbf{\Phi} = \begin{bmatrix} 0 & k_1 & -1 \end{bmatrix}^{\mathrm{T}}$.

Theorem 2: With the control law designed in (17), all signals in the closed-loop system are bounded.

Proof: For the positive definite function defined by $V = e_2^2 / 2,$ one obtains

$$\begin{aligned} \dot{V} &= e_2 \left(k_1 \tilde{x}_2 - \tilde{x}_3 + b u_d + k_1 \hat{x}_2 - k_1 \dot{l}_d \right) \\ &= e_2 \left(\mathbf{\Phi}^T \tilde{x} - \tilde{b} u_{da} - \frac{b}{b \min} k_2 e_2 + b u_{ds2} \right) \\ &\le -\frac{b}{b \min} k_2 e_2^2 + \varepsilon_2 \end{aligned} \tag{20}$$

Under the proposed robust controller based on the LESO, the system is bounded-input bounded-state (BIBS) stable. Furthermore, the positive definite function $V(t)$ is bounded above by

$$V(t) \le V(0) e^{-2\frac{b}{b_{\min}} t} + \frac{\varepsilon_2 b_{\min}}{2b} \left(1 - e^{-2\frac{b}{b_{\min}} t} \right) \tag{21}$$

4 Experimental verification and discussion

Based on the hardware setup of the control system, various experiments with sampling time of 0.001 s are implemented to verify the proposed control algorithm. The comparative experiments between the proposed controller and the PID controller are deployed to demonstrate the good control performance of the proposed algorithm.

4.1 Experiments of single soft actuators

The weight and inner diameter of chamber of the modular fluidic soft actuator are 0.0015 kg and 3 mm respectively, so the parameter b is equal to 4,500 π. The other parameters of the LESO and controller including [ω_0, k_1, k_2] are equal to [200, 400, 105] respectively. A series of experiments on single actuator are carried out to verify the effectiveness of the

proposed controller firstly, and the state changes of the soft actuator in the experiments are shown in the Figure 3.

Figure 3 State of modular soft fluidic actuator, (a) single actuator without load, (b) single actuator with load (see online version for colours)

(a) (b)

Figure 4 Experimental results of step tracking control for chambers of the modular fluidic soft actuator, (a) State of chamber 1, (b) State of chamber 2, (c) State of chamber 3 (see online version for colours)

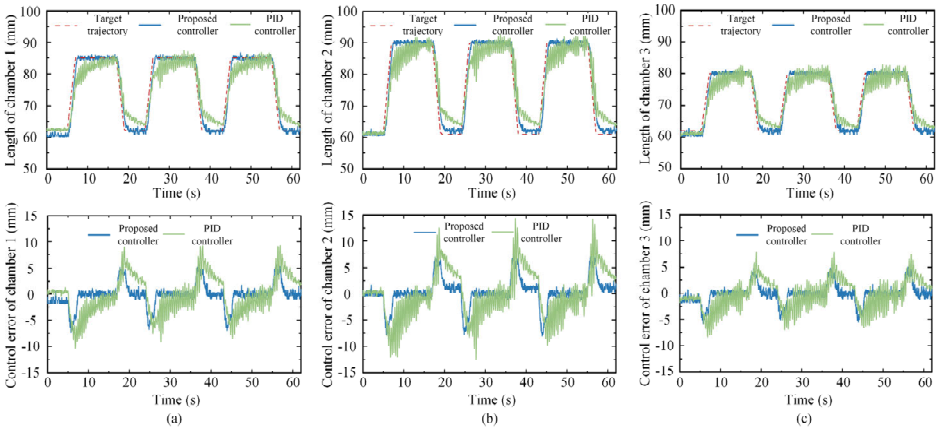

For chamber length control of single soft actuator without load, the comparative experiments between the proposed controller and the PID controller are deployed as shown in Figure 4. The PID gains are tuned by Ziegler–Nichols rule and adjusted furthermore by trial and error to obtain relatively good results. The gains [k_p, k_i, k_d] of the PID controller are set to [0.13, 0.05, 0]. The results indicate that the measured trajectory from the proposed controller closely matches the target trajectory and outperforms the PID controller. It is important to note that although the response of the soft actuator is relatively slow under the PID controller in the experiments, the soft actuator exhibits significant oscillation and large steady-state error, almost failing to reach a steady-state. As a result, it is difficult to achieve better performance using the PID controller, and further quantitative analysis of the experimental results of the PID controller is not pursued. Due to the response delay of the pneumatic proportional valves, there are slight time lags between the experimental data and the target data. The steady control error of the chamber length is below 2 mm and the maximum dynamic control error is about 8

mm under the noise of the visual measurement system by using the proposed controller, which is significantly improved in comparison with the PID controller.

Figure 5 shows the control results of the chamber length of single actuator with a load caused by another actuator, which can be regarded as an external disturbance. In the test, the control input is set to be the same as in the no-load test to validate the dynamic control performance of the controller in the presence of an external load (constant external disturbance) of the soft actuator. It can be observed that the tracking performance such as steady error and dynamic error has no significant degradation compared with non-load experiment, which demonstrates the robustness and efficient active rejection of external disturbance changes.

Figure 5 Experimental results of step tracking control for chambers of the modular fluidic soft actuator with load, (a) State of chamber 1, (b) State of chamber 2, (c) State of chamber 3 (see online version for colours)

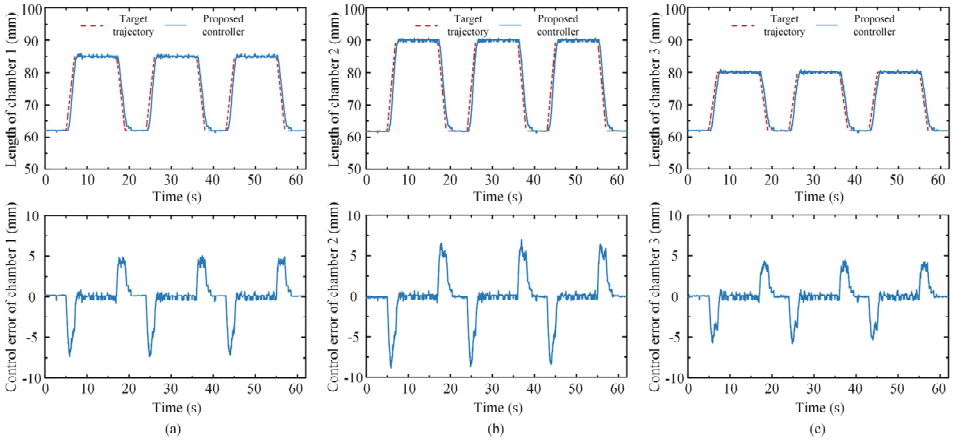

Figure 6 Motion trajectory tracking of single soft actuator, (a) motion state, (b) fluidic pressure (see online version for colours)

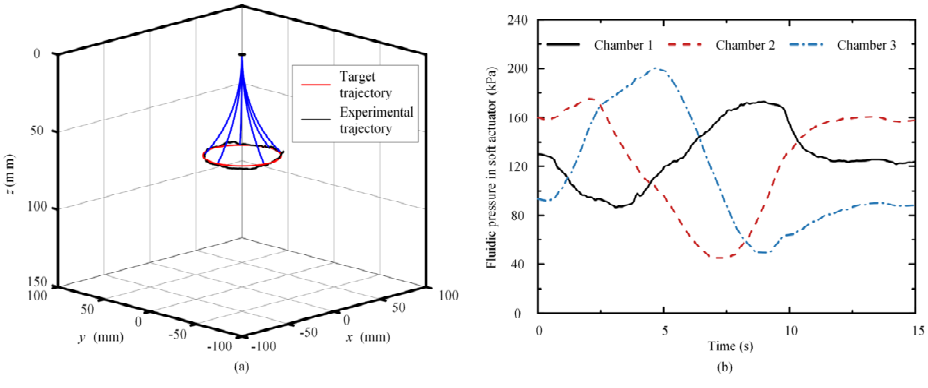

Experiments are also implemented to track a spatial trajectory in order to evaluate the performance of actuator end tracking control. The spatial trajectory is set as a circular trajectory parallel to the horizontal plane with the coordinates of (0, 0, 65) mm as the

centre and 15 mm as the radius in the base coordinate system of the soft actuator. Figure 6 presents the results when the actuator tip tracks a spatial circle trajectory with the radius of 15 mm. It can be seen that the measured trajectory is approximate the same as the target trajectory, and the root mean square error (RMSE) between the experimental data and the desired data is 11.8 mm.

Figure 7 Motion trajectory tracking of two actuators connected in series, (a) motion state, (b) fluidic pressure (see online version for colours)

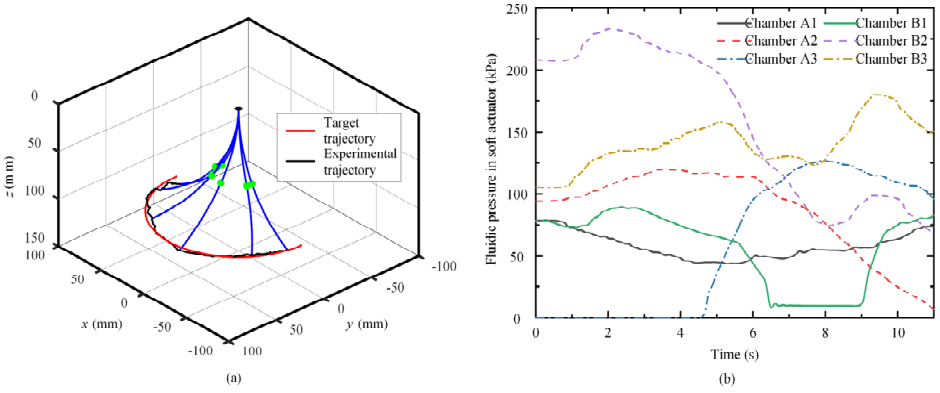

4.2 Experiments of two soft actuators connected in series

To increase the workspace and spatial motion range of the actuator, a large soft actuator is assembled of two modular fluidic soft actuators connected in series.

Further, in order to verify the dynamic control performance when simultaneously controlling two modular fluidic soft actuators, a spatial trajectory tracking experiment with two soft actuators connected in series is implemented. Limited by the measurement range of the vision measurement system, a space semicircle trajectory is designed for the experiment. The centre and radius of the semicircle are equal to (0, 0, 130) and 30 mm respectively. The Figure 7 presents the results when the actuator tip tracks the target trajectory, the green ball in Figure 7(a) represents the end of the upper soft actuator. The experimental result shows that the measured trajectory is approximate the same as the target trajectory, and RMSE between the experimental data and the desired data is 36.2 mm, which proves the good dynamic control performance of the proposed controller. Additionally, the experimental result also shows the applicability of the proposed controller to different actuators and the effectiveness of simultaneous control of multiple modular fluidic soft actuators.

5 Conclusions and future work

This work proposes a robust ADRC method based on the LESO and robust controller to realise effective dynamic control for modular fluidic soft actuators under external disturbance. Experiments including chamber length control and spatial trajectory tracking are implemented for single actuator and two actuators connected in series respectively. The results show that higher robustness and better disturbance rejection ability are

achieved using the proposed controller in comparison to the commonly used PID control method. Furthermore, the proposed controller could provide practical solutions for achieving good control performance of modular fluidic soft actuators in various specific tasks, including marine biological sampling, grasping fragile objects, human-machine interaction operations, and bionic locomotion. With continued research and development, the soft actuators could be utilised in a wide range of applications, ultimately leading to innovative solutions for assisting humanity in a variety of ways.

Acknowledgements

This work was supported by the National Natural Science Foundation of China under Grant No. 51875504, and the Fundamental Research Funds for the Central Universities under Grant No. 226-2023-00049.

References

Abidi, H., Gerboni, G., Brancadoro, M. et al. (2018) 'Highly dexterous 2-module soft robot for intra-organ navigation in minimally invasive surgery', *Int. J. Med. Robot*, February, Vol. 14, No. 1, p.e1875.

Abondance, S., Teeple, C.B. and Wood, R.J. (2020) 'A dexterous soft robotic hand for delicate in-hand manipulation', *IEEE Robotics and Automation Letters*, Vol. 5, No. 4, pp.5502–5509.

Chu, C.Y. (2018) 'Patterson RM. Soft robotic devices for hand rehabilitation and assistance: a narrative review', *J. Neuroeng. Rehabil*., February 17, Vol. 15, No. 1, p.9.

Cianchetti, M., Ranzani, T., Gerboni, G. et al. (2014) 'Soft robotics technologies to address shortcomings in today's minimally invasive surgery: the stiff-flop approach', *Soft Robotics*, Vol. 1, No. 2, pp.122–131.

Fareh, R., Khadraoui, S., Abdallah, M.Y. et al. (2021) 'Active disturbance rejection control for robotic systems: a review', *Mechatronics*, Vol. 80, p.102671.

Feng, H., Sun, Y., Todd, P.A. et al. (2020) 'Body wave generation for anguilliform locomotion using a fiber-reinforced soft fluidic elastomer actuator array toward the development of the eel-inspired underwater soft robot', *Soft Robot*, April, Vol. 7, No. 2, pp.233–250.

Gao, Z. (2003) 'Editor scaling and bandwidth-parameterization based controller tuning 2003: Citeseer', *2003 American Control Conference*, pp.4989–4996.

Gong, Z., Fang, X., Chen, X. et al. (2020) 'A soft manipulator for efficient delicate grasping in shallow water: modeling, control, and real-world experiments', *The International Journal of Robotics Research*, Vol. 40, No. 1, pp.449–469.

Han, J. (2009) 'From PID to active disturbance rejection control', *IEEE Transactions on Industrial Electronics*, Vol. 56, No. 3, pp.900–906.

Hao, L., Xiang, C., Giannaccini, M.E. et al. (2018) 'Design and control of a novel variable stiffness soft arm', *Advanced Robotics*, Vol. 32, No. 11, pp.605–622.

Huang, X., Zhu, X. and Gu, G. (2022) 'Kinematic modeling and characterization of soft parallel robots', *IEEE Transactions on Robotics*, Vol. 38, No. 6, pp.1–15.

Kurumaya, S., Phillips, B.T., Becker, K.P. et al. (2018) 'A modular soft robotic wrist for underwater manipulation', *Soft Robot*, August, Vol. 5, No. 4, pp.399–409.

Kwok, S.W., Morin, S.A., Mosadegh, B. et al. (2014) 'Magnetic assembly of soft robots with hard components', *Advanced Functional Materials*, Vol. 24, No. 15, pp.2180–2187.

Laschi, C., Cianchetti, M., Mazzolai, B. et al. (2012) 'Soft robot arm inspired by the octopus', *Advanced Robotics*, Vol. 26, No. 7, pp.709–727.

Lee, C., Kim, M., Kim, Y.J. et al. (2017) 'Soft robot review', *International Journal of Control, Automation and Systems*, Vol. 15, No. 1, pp.3–15.

Li, G., Ding, Y., Feng, Y. et al. (2019) 'Amesim simulation and energy control of hydraulic control system for direct drive electro-hydraulic servo die forging hammer', *International Journal of Hydromechatronics,* Vol. 2, No. 3, pp.203–225.

Li, H., Cheng, L., Li, Z. et al. (2021) 'Active disturbance rejection control for a fluid-driven hand rehabilitation device', *IEEE/ASME Transactions on Mechatronics*, Vol. 26, No. 2, pp.841–853.

Li, H., Go, G., Ko, S.Y. et al. (2016) 'Magnetic actuated pH-responsive hydrogel-based soft micro-robot for targeted drug delivery', *Smart Materials and Structures*, Vol. 25, No. 2, p.027001.

Maeder-York, P., Clites, T., Boggs, E. et al. (2014) 'Biologically inspired soft robot for thumb rehabilitation', *Journal of Medical Devices*, Vol. 8, No. 2, p.020933.

Marchese, A.D. and Rus, D. (2015) 'Design, kinematics, and control of a soft spatial fluidic elastomer manipulator', *The International Journal of Robotics Research*, Vol. 35, No. 7, pp.840–869.

Marchese, A.D., Komorowski, K., Onal, C.D. et al. (2014) 'Design and control of a soft and continuously deformable 2D robotic manipulation system', *2014 IEEE International Conference on Robotics and Automation (ICRA)*, pp.2189–2196.

Marchese, A.D., Katzschmann, R.K. and Rus, D. (2015a) 'A recipe for soft fluidic elastomer robots', *Soft Robot*, March 1, Vol. 2, No. 1, pp.7–25.

Marchese, A.D., Tedrake, R. and Rus, D. (2015b) 'Dynamics and trajectory optimization for a soft spatial fluidic elastomer manipulator', *The International Journal of Robotics Research*, Vol. 35, No. 8, pp.1000–1019.

Ohta, P., Valle, L., King, J. et al. (2018) 'Design of a lightweight soft robotic arm using pneumatic artificial muscles and inflatable sleeves', *Soft Robot*, April, Vol. 5, No. 2, pp.204–215.

Renda, F., Giorelli, M., Calisti, M. et al. (2014) 'Dynamic model of a multibending soft robot arm driven by cables', *IEEE Transactions on Robotics*, Vol. 30, No. 5, pp.1109–1122.

Roderick, W.R.T., Cutkosky, M.R. and Lentink, D. (2021) 'Bird-inspired dynamic grasping and perching in arboreal environments', *Science Robotics*, December, Vol. 6, No. 61, p.eabj7562.

Rus, D. and Tolley, M.T. (2015) 'Design, fabrication and control of soft robots', *Nature*, 2015 May 28, Vol. 521, No. 7553, pp.467–475.

Satheeshbabu, S., Uppalapati, N.K., Chowdhary, G. et al. (2019) 'Open loop position control of soft continuum arm using deep reinforcement learning', *2019 International Conference on Robotics and Automation (ICRA)*, pp.5133–5139.

Shen, Q., Wang, T., Liang, J. et al. (2013) 'Hydrodynamic performance of a biomimetic robotic swimmer actuated by ionic polymer–metal composite', *Smart Materials and Structures*, Vol. 22, No. 7, p.075035.

Shengda, Y., Wang, T. and Zhu, S. (2021) 'Research on energy consumption of fiber-reinforced fluidic soft actuators', *Smart Materials and Structures*, Vol. 30, No. 2, p.025036.

Shepherd, R.F., Stokes, A.A., Freake, J. et al. (2013) 'Using explosions to power a soft robot', *Angew. Chem. Int. Ed. Engl.,* March 4, Vol. 52, No. 10, p.2892-6.

Thuruthel, T.G., Falotico, E., Renda, F. et al. (2019) 'Model-based reinforcement learning for closed-loop dynamic control of soft robotic manipulators', *IEEE Transactions on Robotics*, Vol. 35, No. 1, pp.124–134.

Truby, R.L. and Li, S. (2020) 'Integrating chemical fuels and artificial muscles for untethered microrobots', *Sci. Robot*, August 19, Vol. 5, No. 45, p.eabd7338.

Villanueva, A., Smith, C. and Priya, S. (2011) 'A biomimetic robotic jellyfish (robojelly) actuated by shape memory alloy composite actuators', *Bioinspir Biomim*, September, Vol. 6, No. 3, p.36004.

Wang, T. and Zhang, X. (2022) 'A static modeling approach for thin-walled soft robotic arms considering geometric and material nonlinearity', *IEEE Robotics and Automation Letters*, Vol. 7, No. 2, pp.1832–1839.

Wang, T., Zhang, Y., Chen, Z. et al. (2019a) 'Parameter identification and model-based nonlinear robust control of fluidic soft bending actuators', *IEEE/ASME Transactions on Mechatronics*, Vol. 24, No. 3, pp.1346–1355.

Wang, T., Zhang, Y., Zhu, Y. et al. (2019b) 'A computationally efficient dynamical model of fluidic soft actuators and its experimental verification', *Mechatronics*, Vol. 2019, No. 58, pp.1–8.

Wang, P., Tang, Z., Xin, W. et al. (2022a) 'Design and experimental characterization of a push-pull flexible rod-driven soft-bodied robot', *IEEE Robotics and Automation Letters*, Vol. 7, No. 4, pp.8933–8940.

Wang, T., Zhang, Y., Zhu, Z. et al. (2022b) 'An electrohydraulic control device with decoupling effect for three-chamber soft actuators', *IEEE/ASME Transactions on Mechatronics*, Vol. 27, No. 3, pp.1683–1691.

Wen, J., Wang, G., Jia, J. et al. (2023) 'Compliance control method for robot joint with variable stiffness', *International Journal of Hydromechatronics*, Vol. 6, No. 1, pp.45–58.

Xie, Q., Wang, T. and Zhu, S. (2020b) 'Simplified dynamical model and experimental verification of an underwater hydraulic soft robotic arm', *Smart Materials and Structures*, Vol. 31, No. 7, p.075011.

Xie, Q., Wang, T., Yao, S. et al. (2020a) 'Design and modeling of a hydraulic soft actuator with three degrees of freedom', *Smart Materials and Structures*, Vol. 29, No. 12, p.125017.

Xu, F., Wang, H., Au, K.W.S. et al. (2018) 'Underwater dynamic modeling for a cable-driven soft robot arm', *IEEE/ASME Transactions on Mechatronics*, Vol. 23, No. 6, pp.2726–2738.

Zhang, Y., Wang, T., He, W. et al. (2023) 'Human-powered master controllers for reconfigurable fluidic soft robots', *Soft Robotics*.

Zhang, Y., Yang, D., Yan, P. et al. (2022) 'Inchworm inspired multimodal soft robots with crawling, climbing, and transitioning locomotion', *IEEE Transactions on Robotics*, Vol. 38, No. 3, pp.1806–1819.

Zheng, Q. and Gao, Z. (2018) 'Active disturbance rejection control: some recent experimental and industrial case studies', *Control Theory and Technology*, Vol. 16, No. 4, pp.301–313.

Zhou, Y., Headings, L.M. and Dapino, M.J. (2022) 'Modeling of fluidic prestressed composite actuators with application to soft robotic grippers', *IEEE Transactions on Robotics*, Vol. 38, No. 4, pp.2166–2178.

Zongxing, L., Wanxin, L. and Liping, Z. (2020) 'Research development of soft manipulator: a review', *Advances in Mechanical Engineering*, Vol. 12, No. 8, p.1687814020950094.

Zou, J., Lin, Y., Ji, C. et al. (2018) 'A reconfigurable omnidirectional soft robot based on caterpillar locomotion', *Soft Robot*, April, Vol. 5, No. 2, pp.164–174.